Impact of three-dimensional geometry on the performance of isolated electron-injection infrared detectors

Vala Fathipour, Sung Jun Jang, Iman Hassani Nia, and Hooman Mohseni

Citation: Applied Physics Letters **106**, 021116 (2015); doi: 10.1063/1.4905864
View online: http://dx.doi.org/10.1063/1.4905864
View Table of Contents: http://scitation.aip.org/content/aip/journal/apl/106/2?ver=pdfcov
Published by the AIP Publishing

Impact of three-dimensional geometry on the performance of isolated electron-injection infrared detectors

Vala Fathipour, Sung Jun Jang, Iman Hassani Nia, and Hooman Mohseni[a)]
Bio-Inspired Sensors and Optoelectronics Laboratory, Northwestern University, 2145 Sheridan Rd, Evanston, Illinois 60208, USA

(Received 30 September 2014; accepted 27 December 2014; published online 15 January 2015)

We present a quantitative study of the influence of three-dimensional geometry of the isolated electron–injection detectors on their characteristics. Significant improvements in the device performance are obtained as a result of scaling the injector diameter with respect to the trapping/absorbing layer diameters. Devices with about ten times smaller injector area with respect to the trapping/absorbing layer areas show more than an order of magnitude lower dark current, as well as an order of magnitude higher optical gain compared with devices of same size injector and trapping/absorbing layer areas. Devices with 10 μm injector diameter and 30 μm trapping/absorbing layer diameter show an optical gain of ~2000 at bias voltage of −3 V with a cutoff wavelength of 1700 nm. Analytical expressions are derived for the electron-injection detector optical gain to qualitatively explain the significance of scaling the injector with respect to the absorber. © *2015 AIP Publishing LLC*. [http://dx.doi.org/10.1063/1.4905864]

Sensitive short-wavelength infrared (SWIR) detectors with ultra low noise levels and high signal-to-noise ratios are highly desirable to allow detection of signal levels down to few photons.[1,2] Such detectors are currently the performance bottleneck in new scientific fields of research such as quantum information science and quantum key distribution.[3] Furthermore, they are largely beneficial to a wide range of applications including astronomy,[4] biophotonics,[5] optical tomography,[6] Light Detection and Ranging (LIDAR),[7] and nondestructive material evaluation.[8]

Mainstream InGaAs PIN detectors have extremely low dark current. However, the absence of internal amplification in these detectors places stringent conditions on the read-out integrated circuit (ROIC) noise levels and below ~−20 °C the imager becomes limited by the ROIC noise.

Thus, to allow ultimate sensitivity, the detector signal should not only surpass the detector noise, but also the electronic noise of the ROIC and hence, having a high internal amplification in addition to a low noise level is highly desirable. Electron-injection detectors are based on a new single photon detection mechanism and address both above criterion.[9–11,19] They operate in linear-mode at low bias voltages and provide a large internal avalanche-free amplification with an excess noise factor of near unity.[11] Furthermore, they can be formed into compact imagers[9] and are made with the mature and low-cost InP material system. Our previous results reported characteristics of un-isolated detectors with large dark currents (6 μA at −1.5 V bias), which prevented long integration times in the camera.[9]

Recently, we have isolated individual detector active regions from each other to address the large device dark current.[12–16,18] Characteristics of the isolated devices and comparisons to the previously reported results are provided in Refs. 13–16. In this paper, we illustrate the benefit of scaling of the injector with respect to the trapping/absorbing layer areas in isolated devices. We then develop an analytical model based on heterojunction transistors,[17,27] to qualitatively explain the measured optical gain (G_{opt}) improvement in a scaled injector device.

Schematic diagram as well as Scanning Electron Microscope (SEM) image of the isolated electron-injection detector with 10 μm injector and 30 μm trapping/absorbing layer diameters are shown in Figs. 1(a) and 1(b), respectively. Layer structure is composed of 1000 nm of n^- doped $In_{0.53}Ga_{0.47}As$ absorber, 50 nm of p^+ doped $GaAs_{0.52}Sb_{0.48}$ trapping layer, 50 nm of undoped $In_{0.52}Al_{0.48}As$ etch-stop

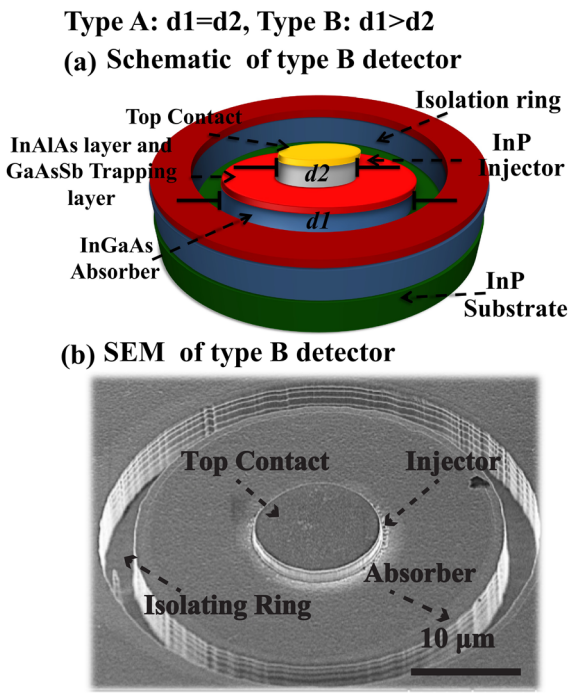

FIG. 1. (a) Schematic diagram and (b) SEM of type B electron-injection detector with 10 μm injector diameter and 30 μm absorber diameter. *d1* and *d2* refer to the trapping/absorbing layer and injector diameters, respectively.

[a)]hmohseni@northwestern.edu

layer, 500 nm of n^+ doped InP injector, and 50 nm n^+ doped $In_{0.53}Ga_{0.47}As$ cap layer. Layers are grown by metal organic chemical vapor deposition on 2-in. InP substrates.[18]

To study the impact of scaling of the injector with respect to the trapping/absorbing layer areas, two types of detector geometries were fabricated: type A detectors have mesa structures with equal trapping/absorbing layer diameter (d1) and injector diameter (d2) and type B detectors have a smaller injector diameter compared with the trapping/absorbing layer diameter. To fabricate devices, wafers were patterned to define the contacts. Conventional metal evaporation and a lift-off method were used to define the multi-layer metal contacts. For type A detector formation, the wafer was then patterned and wet etched to create the mesas. For type B detector formation, after the contact metal lift-off step, dry etching was performed to form the injector pillars using the metal contacts as hard mask. Wafers were then patterned for isolating trenches, which were formed with a combination of wet etching and dry etching. Different sizes of both detector types were fabricated. For type A detectors, d1 = d2 varied between 274 μm, 174 μm, 123 μm, 82 μm, and 33 μm, and for type B detectors, injector diameter was 10 μm and the trapping/absorbing layer diameter was 30 μm. Our current probing method for electrical measurements does not allow reliable results for contact diameters below 10 μm.

For photo-response measurement, a calibrated continuous wave laser source with a peak emission wavelength at 1550 nm and ~10 μm spot size was used to illuminate devices from the backside. Laser power was calibrated using a calibrated PIN detector. It must be mentioned that our previous experimental results show that the generated electron-hole pair are immediately removed from the active layer (psec).[19] Thus for laser spot sizes smaller than the active region, the measured quantum efficiency and the optical gain are independent of the beam size.

Fig. 2(a) shows the measured dark current versus bias voltage characteristic for type A and type B devices at room temperature. To obtain statistically correct data, for each detector type, dark current of an average number of 10 devices was measured per device size. Dark current of type A detectors with mesa sizes ≥80 μm scales proportional with the device area and follows the expected sub-linear relation with bias voltage.[16] Dark current of the scaled injector type B device is an order of magnitude lower than that of a type A device with a similar mesa size (33 μm mesa).

Detector responsivity was obtained from dark and photocurrent measurements. External quantum efficiency was calculated from the uncoated surface reflectivity, the thickness of the absorbing layer, and its absorption coefficient and estimated as 78%. Fig. 2(b) shows the extracted optical gain, (G_{Max}), at tens of micro watts of optical power, versus bias voltage for type A and type B devices at room temperature. Optical gain increases with bias at small negative bias voltages, and beyond bias voltage of ~−1.5 V a stable gain of ~100 for type A devices and ~2000 for type B device is achieved. From Figs. 2(a) and 2(b), one can conclude that the internal dark current densities (obtained by dividing the external dark current densities by the optical gain) of all device structures have similar values with the exception of the smallest mesa type A device, which may possibly be

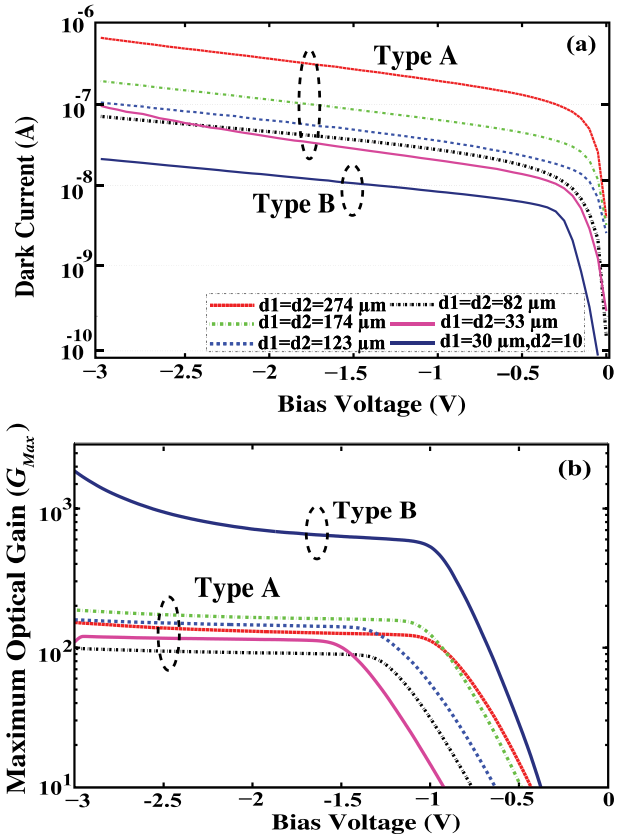

FIG. 2. (a) Measured electron-injection detector dark current versus bias voltage characteristic. Data were obtained by averaging over 10 detectors per device size. (b) Measured optical gain, (G_{Max}), at tens of micro watts of optical power, versus bias voltage characteristic. Color-coding for part (a) and (b) is the same.

dominated by surface effects. The surface effects seem to be not very significant despite the rather large exposed surfaces in the type B devices.

Optical gain was measured at room temperature for various incident optical power levels in both types of detectors. The corresponding plot of the measured optical gain versus the photogenerated current density at −3 V bias voltage is shown in Fig. 3. Optically generated holes are trapped in the GaAsSb trapping layer and their accumulation causes an

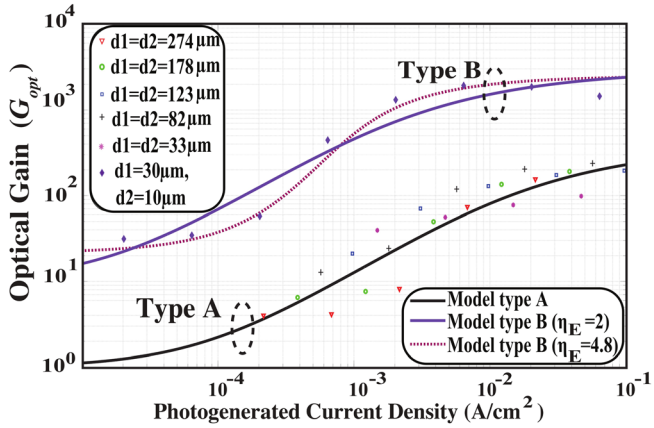

FIG. 3. Optical gain as a function of the photogenerated current density at −3 V bias voltage: Markers show the measured data and the solid lines show our developed analytical model. Good match to data of type B device is obtained for η_E = 4.8. This may be an indication of the defects at the hetero-junction.[31] All measurements in this figure are performed at room temperature.

increase in the forward bias voltage (V_{BE}) of the injector/trapping layer heterojunction. To derive an analytical expression for the optical gain, the device is assumed to be operating in the forward operation regime. Both the photogenerated current, I_{gen}, Eq. (1) and the resulting amplified photo current injected from the injector into the absorber, $I_{amp-photo}$, Eq. (2) are driven by the forward bias voltage[27]

$$I_{gen} = I_S\left[(\gamma^{-1})\left[e^{\frac{qV_{BE}}{\eta_F KT}}-1\right]+\left(\frac{I_{SS}}{I_S}\right)\left[e^{\frac{qV_{BE}}{\eta_F KT}}-1\right] + \frac{I_{SE}}{I_S}\left[e^{\frac{qV_{BE}}{\eta_E KT}}-1\right]\right], \quad (1)$$

$$I_{amp-photo} = I_S\left[e^{\frac{qV_{BE}}{\eta_F KT}}-1\right], \quad (2)$$

where $I_S = q\frac{D_n}{Wp}A_B\frac{{n_{iP}}^2}{N_{pA}}$ is the saturation current injected to the absorber, I_{SS} is the saturation current for recombination in the undepleted part of GaAsSb layer, and I_{SE} is the saturation current for recombination in injector/trapping layer space charge region primarily at low optical power levels. This current is more significant than I_{SS} and is usually large in heterojunction devices due to the strong and dominant recombination in the base emitter space charge region.[20–22,26,27] As we shall see shortly, scaling of the injector with respect to the trapping layer reduces this recombination current ideally by the ratio of trapping layer to injector area (A_B/A_E). The factor $\gamma^{-1} = \frac{D_p}{D_n}\frac{W_p}{W_n}\frac{N_{pA}}{N_{nD}}\left(\frac{{m_{en}}^* {m_{hn}}^*}{{m_{ep}}^* {m_{hp}}^*}\right)^{\frac{3}{2}} e^{\frac{E_{gp}-E_{gn}}{KT}}$ represents the ratio of (hole) minority carrier injection to InP, to (electron) majority carrier injection to GaAsSb. In the expression for γ^{-1}, D_n and D_p are the minority carrier diffusion coefficients in GaAsSb and InP layers, W_p and W_n are the respective layer thicknesses, and N_{pA} and N_{nD} are the doping concentrations (acceptor and donor, respectively). Furthermore, ${m_{ep}}^*$, ${m_{hp}}^*$ and ${m_{en}}^*$, ${m_{hn}}^*$ are the effective masses of electron and hole in GaAsSb and InP layers and E_{gp} and E_{gn} are the relative bandgap energies. In the expression for I_S, n_{iP} is the GaAsSb intrinsic carrier concentration and in Eqs. (1) and (2), η_F and η_E are the injector and trapping layer current ideality factors. Using published experimental parameters given in Refs. 23–25, we find $\gamma = 2.95\text{x}10^{10}$. Under large optical power levels (tens of micro watts), optical gain, which is the ratio of $I_{amp-photo}$ to I_{gen} has maximum value of "$G_{Max} \sim \frac{I_{amp-photo}}{I_{gen}}|_{Max} \sim \frac{1}{[(\gamma^{-1})+(I_{SS}/I_S)]}$" and its value can be read from measurement data of Fig. 2(b) or Fig. 3.

Using G_{Max} in Eqs. (1) and (2), optical gain can be expressed as

$$G_{opt} = \frac{I_{amp-photo}}{I_{gen}} = \frac{G_{Max}\left[e^{\frac{qV_{BE}}{\eta_F KT}}-1\right]}{\left[e^{\frac{qV_{BE}}{\eta_F KT}}-1\right]+G_{Max}\ \frac{J_{SE}}{J_S}\ \frac{A_E}{A_B}\left[e^{\frac{qV_{BE}}{\eta_E KT}}-1\right]}, \quad (3)$$

where $I_S = A_B J_S$ and $I_{SE} = A_E J_{SE}$. Assuming that the effective cross section of saturation current I_S is related to the base area A_B, we get a good fit to our measurement data. Using Eq. (3), curves were fitted to measurement data for type A and type B devices (Fig. 3). The corresponding values used to obtain the curves are presented in Table I, where the first three rows show the constants and the last three rows show the fitting parameters. Although the epitaxial structures are the same, the slight difference in the value of J_S for type A and type B devices might be the result of possible variation in the epitaxial growth (e.g., actual doping levels, thicknesses, and compositions). Furthermore, it has been assumed that the recombination current in the depletion region dominates the surface/defect components in the injector/trap heterojunction, i.e., $\eta_E = 2$. Measurement data together with Eq. (3) suggest both higher optical gain and lower photogenerated current density for the gain drop in the type B devices. These are possibly the result of a reduced recombination current in the injector/trap depletion region of a scaled injector device. Similar behavior has also been observed in heterojunction bipolar phototransistors.[26]

TABLE I. Values used in plot of Fig. 3: first 3 rows show the constants and the last 3 rows show the fitting parameters used to obtain the curves.

Variables	Type A	Type B
A_E/A_B	1	1/9
η_E	2	2
η_F	1	1
G_{Max}	400	3000
J_{SE}/J_S	2	2
J_S (A cm^{-2})	2×10^{-5}	4×10^{-5}

A common issue with heterojunction phototransistors is the reduction of gain at low optical powers. The gain in such devices drops to half of its peak value at photogenerated current density values of $\sim 10^0 - 10^{-2}$ Acm^{-2},[27–29] which is similar to the measured values in the type A devices. However, this value is pushed back by at least one order of magnitude in the type B devices (see Fig. 3). Our model together with the measurement results suggest that scaling of the emitter with respect to the base in such devices could possibly address this issue.

Another interesting observation is that the assumption of $\eta_E = 2$ (i.e., the typical ideality factor for generation recombination (GR)-limited condition) results in a slope of $m \sim 0.7$ for the optical gain drop versus photogenerated current density. This is considerably less than the slope of measurement data ($m \sim 1$) for the type B device. Note that a similar slope (i.e., $m \sim 1$) is also observed for a device with comparable structure.[30] A better fit to the measurement data could be obtained using $\eta_E = 4.8$ in Eq. (3), (dashed line in Fig. 3). It is possible that defects at the heterojunction[31] contribute to such large η_E values.

In conclusion, we have systematically studied the effect of 3D geometry on the isolated electron-injection detector's dark current and gain characteristics. Two different detector geometries were fabricated: type A geometry with same size injector and trapping/absorbing layer diameters and type B geometry with a smaller injector than the trapping/absorbing layer diameters. Dark current of the type B device is an order of magnitude lower than that of a type A device with a similar mesa size (33 μm mesa). Furthermore, experimental

measurement data together with the developed analytical model confirm that the type B device presents a larger optical gain and maintains the large optical gain down to a lower illumination level. This was affiliated with the lower recombination current in the GaAsSb/InP space charge region for the type B geometry. For example, it was experimentally shown that ~ten times reduction of injector area compared with the trapping/absorbing layer areas results in more than ten times improvement in the optical gain, which is maintained down to ~ten times lower optical power densities. This improvement may be further enhanced with smaller A_E/A_B ratio.

We acknowledge partial support from DARPA/ARO Award Nos. W911NF-11-1-0390 and W911NF-12-1-0324 and W911NF-13-1-0485, as well as NSF Award No. ECCS-1310620. One of the authors (V.F.) would also like to acknowledge Ryan Fellowship support. We would like to acknowledge the use of Argonne National Laboratory Center for Nanoscale Materials. Use of the Center for Nanoscale Materials was supported by the U.S. Department of Energy, Office of Science, Office of Basic Energy Sciences, under Contract No. DE-AC02-06CH11357.

[1]A. Rogalski, Infrared Phys. Technol. **54**, 136 (2011).
[2]G. Vojettaa, F. Guelleca, L. Mathieua, K. Fouberta, P. Feautrierb, and J. Rothmana, Proc. SPIE **8375**, 83750Y (2012).
[3]A. L. Migdall and J. P. Dowling, "Introduction to *journal of modern optics* special issue on single-photon: Detectors, applications, and measurement methods," J. Mod. Opt. **51**, 1265–1266 (2004).
[4]M. MacDougal, J. Geske, C. Wang, S. Liao, J. Getty, and A. Holmes, Proc. SPIE **7298**, 72983F (2009).
[5]A. Demarco, A. Periasamy, C. F. Booker, and R. N. Day, Nat. Methods **3**, 519 (2006).
[6]Y. Du, X. H. Hu, M. Cariveau, X. Ma, G. W. Kalmus, and J. Q. Lu, Phys. Med. Biol. **46**, 167 (2001).
[7]A. Pasmanik, E. J. Shklovsky, G. I. Freidman, V. V. Lozhkarev, A. Z. Matveyev, A. A. Shilov, I. V. Yakovlev, D. G. Peterson, and J. K. Partin, Proc. SPIE **3065**, 286 (1997).
[8]E. Diamanti, C. Langrock, M. M. Fejer, Y. Yamamoto, and H. Takesue, Opt. Lett. **31**, 727 (2006).
[9]O. G. Memis, J. Kohoutek, W. Wu, R. M. Gelfand, and H. Mohseni, IEEE Photonics J. **2**, 858 (2010) (Fig. 5., pp. 862).
[10]O. G. Memis, A. Katsnelson, S. C. Kong, H. Mohseni, M. Yan, S. Zhang, T. Hossain, N. Jin, and I. Adesida, Appl. Phys. Lett. **91**, 171112 (2007).
[11]O. G. Memis, A. Katsnelson, S. C. Kong, H. Mohseni, M. Yan, S. Zhang, T. Hossain, N. Jin, and I. Adesida, Opt. Express **16**, 12701 (2008).
[12]V. Fathipour, S. J. Jang, R. Brown, and H. Mohseni, "Highly sensitive and linear electron-injection detectors at the telecomm wavelength," in Frontiers in Optics (FiO), Tucson, Arizona, USA (2014).
[13]V. Fathipour, O. G. Memis, S. J. Jang, R. Brown, and H. Mohseni, in ISDRS 2013 International Semiconductor Device Research Symposium Maryland, 11–13 December 2013.
[14]V. Fathipour, S. J. Jang, I. Hassaninia, and H. Mohseni, Proc. SPIE **9220**, 92200J–92200J-6 (2014).
[15]V. Fathipour, S. J. Jang, and H. Mohseni, "New generation of isolated electron-injection imagers," IEEE 13th Workshop on Information Optics (WIO), page 1–3, Neuchatel, Switzerland (2014).
[16]V. Fathipour, O. G. Memis, S. J. Jang, R. L. Brown, I. Hassani Nia, and H. Mohseni, "Isolated electron injection detectors with high gain and record low dark current at telecom wavelength," IEEE J. Sel. Top. Quantum Electron. **20**(6), 3805106 (2014).
[17]M. E. Hafizi, C. R. Crowell, and M. E. Grupen, IEEE Trans. Electron Devices **37**, 2121 (1990).
[18]V. Fathipour, O. G. Memis, S. J. Jang, F. Khalid, R. Brown, I. HassaniNia, R. M. Gelfand, and H. Mohseni, Proc. SPIE **8868**, 886803 (2013).
[19]O. G. Memis, A. Katsnelson, H. Mohseni, M. Yan, S. Zhang, T. Hossain, N. Jin, and I. Adesida, IEEE Electron Device Lett. **29**, 867 (2008).
[20]J. C. Campbell and K. Ogawa, J. Appl. Phys. **53**, 1203 (1982).
[21]S. W. Tan, W. T. Chen, M. Y. Chu, and W. S. Lour, in *Junction Technology*, IWJT '04, 2004, p. 232.
[22]S. Chandrasekhar, M. K. Hoppe, A. G. Dentai, C. H. Joyner, and G. J. Qua, IEEE Electron Device Lett. **12**, 550 (1991).
[23]E. W. Iverson, T. S. Low, B. R. Wu, M. Iwamoto, and D. D'Avanzo, CS MANTECH Conference, Denver, Colorado USA (2014).
[24]C. Maneux, M. Belhaj, B. Grandchamp, and N. Labat, Solid State Electron. **49**(6), 956 (2005).
[25]See http://www.ioffe.ru/SVA/NSM/ for the experimental parameters used for the calculation of the ratio of minority carrier injection to InP, to majority carrier injection to GaAsSb in Eq (3).
[26]M. S. Park, D. S. Kim, and J. H. Jang, International Conference on Indium Phosphide and Related Materials (IPRM) (2010).
[27]C. C. Lin, W. Martin, J. S. Harris, Jr., and F. Sugihwo, Appl. Phys. Lett. **76**, 1188 (2000).
[28]J. C. Campbell, A. G. Dentai, C. A. Burrus, Jr., and J. F. Ferguson, IEEE J. Quantum Electron. **17**, 264 (1981).
[29]J. C. Campbell, C. A. Burrus, A. G. Dentai, and K. Ogawa, Appl. Phys. Lett. **39**, 820 (1981).
[30]M. S. Park and J. H. Jang, IEEE Photonics Technol. Lett. **22**, 1202 (2010).
[31]M. Konagai and K. Takahashi, J. Appl. Phys. **46**, 2120 (1975).